Chapter 2

Optical Fibre Sensors Based on UV Inscribed Excessively Tilted Fibre Grating

Chengbo Mou, Zhijun Yan, Kaiming Zhou and Lin Zhang

Additional information is available at the end of the chapter

http://dx.doi.org/10.5772/57146

1. Introduction

In-fibre inscription of grating structures in the core of an optical fibre was firstly reported in 1978 by Hill [1]. Being a promising device as narrow band reflector, the fibre Bragg gratings (FBGs) have drawn a lot of attentions in the field of optical communication at that time. However, the functionality of FBGs as sensors has been only recognised after a decade of the invention of the device which can inscribe FBG with resonant wavelength independent of the writing laser wavelength [2]. Since then, the research of FBG based sensors has grown tremendously [3]. The techniques using diffractive optical element to fabricate FBG have put the field into a more commercial way as reproductive of identical FBGs is possible [4]. FBGs are then found a range of applications in sensing field such as strain, temperature, curvature, loading, displacement etc. In 1996, a new type of fibre grating device which is called long period fibre grating (LPG) was demonstrated which has superior temperature sensitivity while possessing refractive index (RI) responsivity [5]. Both FBGs and LPGs have shown significant role in the optical sensing domain. They have been utilised directly or functionalised or integrated with other structures to show functionality in various sensing applications.

Another class of in-fibre gratings is the grating structure with tilted grating planes which called tilted fibre gratings (TFGs). Such a type of gratings is capable of couple the core propagating mode into strong cladding modes. In terms of the tilted angles, such gratings can be divided into three types namely small angle (<45°) TFG, 45° TFG and excessively (>45°) TFG (ETFG). The small angle TFGs were originally used as mode coupler which taps the light out from the fibre core area [6]. Recently, such gratings have shown strong potential in sensing field [7-10]. When incorporated with metal coating, such gratings also exhibit great potential for refractive index sensing based on surface plasmon resonance [11]. 45°-TFG was initially demonstrated

INTECH
open science | open minds

© 2014 The Author(s). Licensee InTech. This chapter is distributed under the terms of the Creative Commons Attribution License (http://creativecommons.org/licenses/by/3.0), which permits unrestricted use, distribution, and reproduction in any medium, provided the original work is properly cited.

as a polarisation dependent loss equaliser [12] and later as an in-fibre polariser [13]. The ETFG is a new class of fibre gratings which was first demonstrated in 2006 by Zhou *et al* [14]. Since then, the ETFGs have shown great capability as a novel kind of fibre sensors. This chapter will review the recent development of ETFGs as various optical sensors. The chapter will be organised in three main parts: first part (sections 2) gives a general introduction and fundamental background on fibre gratings with a particular emphasis on the ETFG; second part (section 3) describes the inscription and characterisation of ETFG; third part (sections 4-9) discusses ETFG based sensors and fibre laser sensing systems including strain, twist [15, 16], loading[17], refractive index (RI) and liquid level sensing [18].

2. Background of fibre gratings

Light coupling in a non-tilted fibre grating can be well illustrated by ray tracing as shown in Figure 1. For an FBG, the mode coupling occurs at resonant wavelength where the forward propagating mode reflects into an identical backward propagating mode (Figure 1a). While for an LPG, the mode coupling occurs close to wavelength at which a forward propagating core mode is strongly coupled into co-propagating cladding modes (Figure 1b). For TFGs, the mechanism of light coupling can also be described by ray tracing method as shown in Figure 2.

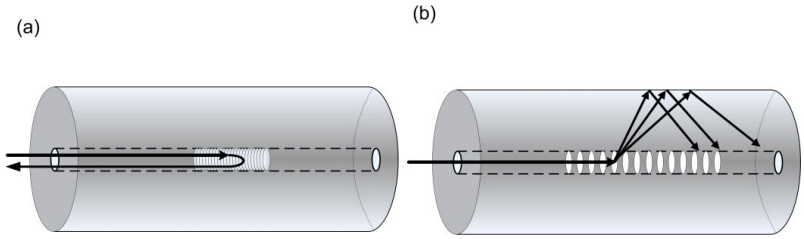

Figure 1. Schematic of light coupling of (a) a FBG showing light coupled from forward propagating core mode to backward propagating cladding mode; (b) a LPG showing light coupled from forward propagating core mode to forward propagating cladding modes.

As can be seen from Figure 2, when the grating tilted angle is smaller than 45°, the grating is capable of coupling forward propagating core mode into backward propagating cladding modes (Figure 2a). At 45°, as a unique case, the core mode will be coupled into radiation mode normal to the fibre axis (Figure 2b). When the tilted angle is larger than 45°, like LPGs, the ETFGs are capable of coupling the forward propagating core mode into forward propagating cladding modes, but to the high order ones (Figure 2c). The strongest light coupling occurs at the resonant wavelength where the phase matching condition $\lambda_{co\text{-}cl}=(n_{c0}\pm n_{cl,m})\ \Lambda/\cos\theta$ is satisfied, where n_{c0} and $n_{cl,m}$ are the effective mode refractive indices of the core mode and the mth cladding mode, Λ is the grating period and θ is the tilted angle of the grating structure. The mode coupling mechanism can be well understood by the phase matching condition. We hereby define the following wave vector relationship for mode coupling in a fibre grating

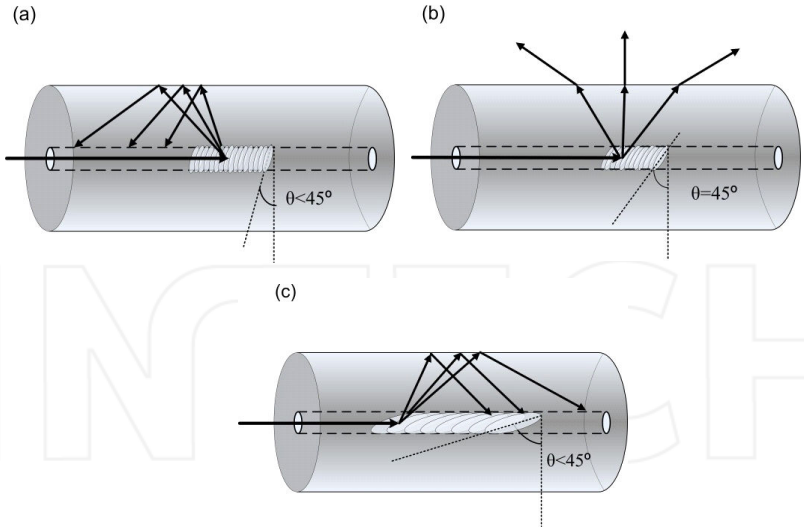

Figure 2. Schematic of light coupling of TFGs with tilted angle (a)< 45°; (b)=45°;(c)>45°.

which is commonly regarded as the phase matching condition $K_{out} = K_{in} + K_G$. All K described in this section are vectors. $K_{in} = \frac{2\pi}{\lambda} \cdot n_{co}$ is the wave vector of the incident light and $K_G = \frac{2 \cdot \pi}{\Lambda_G}$ is the grating vector. The phase matching condition of a fibre grating can then be described in a vectorial plane in Figure 3 and Figure 4. For the case of FBG mode coupling, as shown in Figure 3a, the relationship $K_{out} = K_{in} = \frac{2 \cdot \pi}{\lambda} \cdot n_{co}$ applies as an FBG structure will couple the light from a forward propagating core mode into an identical backward propagating core mode. For the case of LPG mode coupling, as shown in Figure 3b, the grating can couple the incident light into forward propagating cladding modes with $K_{out} = \frac{2\pi}{\lambda} \cdot n_{cl}$ indicating the cladding modes.

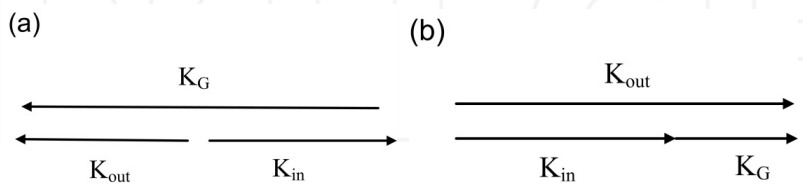

Figure 3. Vectorial descriptions of phase matching conditions of (a) FBG and (b) LPG.

For TFGs, as the grating has the ability to couple the forward propagating core mode into radiation mode, it is hence to have $K_{out} = \frac{2 \cdot \pi}{\lambda} \cdot n_{clad}$ which is similar to LPG. With the condition

$n_{co} \cong n_{clad}$, the following relationship $K_{in} \cong K_{out}$ therefore applies. Hence, the phase matching condition of TFGs can be depicted in the vector plane which is shown in Figure 4, where θ indicates the tilted angle of the grating with respect to the fibre axis. In Figure 4a, we can simply infer that when the tilted angle is minimised to zero, the phase matching illustration evolves into the standard FBG condition from which a forward propagating mode has been coupled into an identical backward propagating mode via Bragg diffraction. Figure 4b shows the special case of 45°-TFG which is capable of coupling out light perpendicular to the fibre axis or incident beam propagation direction. While Figure 4c shows the mechanism of an incident beam couples into a forward propagating mode through an excessively titled grating structure. Although the phase matching condition gives very good approximation for interpretation of mode coupling mechanism inside the TFGs, it does not involve the polarisation effect which is actually one of the key properties of the TFGs.

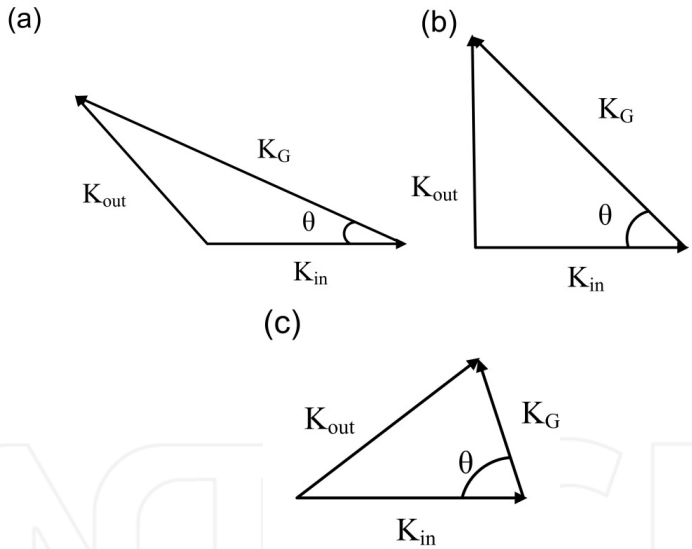

Figure 4. Vectorial description of phase matching conditions for TFGs with titled angles at (a) < 45°, (b) = 45° and (c) > 45°.

Due to their large tilted angle induced strong asymmetry to the fibre geometry, ETFGs exhibit polarisation dependent mode splitting which features with pairs of peaks corresponding to two orthogonal polarisation modes. We can therefore identify an equivalent fast-axis and slow-axis similar to the conventional polarisation maintaining (PM) fibre structure as shown in Figure 5. It is this distinctive polarisation mode splitting mechanism makes ETFGs as ideal loading [17] and twisting sensors [16] based on their polarisation property and as refractive index sensors utilising intrinsic sensitivity of the high order modes to surrounding medium.

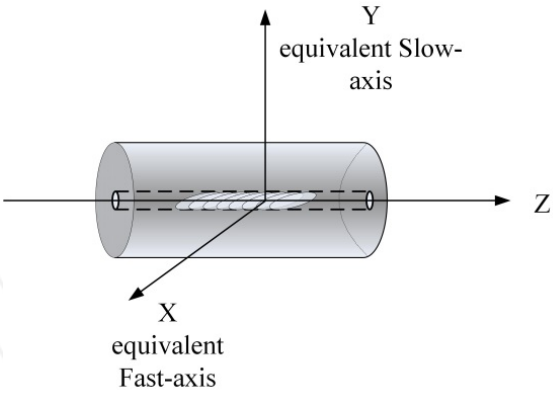

Figure 5. Schematic illustration of an ETFG structure with two assigned orthogonal polarisation axes.

3. Fabrication and spectral properties of ETFG

As illustrated in Figure 6, a TFG can be inscribed either by tilting the mask with respect to the fibre axis (Figure 6a), or by using a mask with tilted pitches (Figure 6b). As an alternative approach, one can inscribe such gratings by tilting the fibre about its axis orthogonal to the plane defined by the two interfering UV beams in a two-beam holographic fabrication system (Figure 6c). A commercial argon ion UV laser is employed to inscribe ETFG in hydrogenated standard telecom fibre (SMF28). Similar to standard FBG fabrication, we have adopted mask scanning technique for ETFG inscription due to high reproducibility and fine control of the grating devices. A commercial amplitude mask with 6.6 μm period was purchased for ETFG inscription ensuring the spectral response residing within a broad range from 1200 to 1700 nm. The schematic UV inscription setup is shown in Figure 7a. A typical microscopic image of an ETFG is shown in Figure 7b demonstrating the slanted grating fringes at ~78°.

A broadband light source (BBS), a polariser and a polarisation controller (PC) are utilised to examine the spectral properties of ETFG through an optical spectrum analyser (OSA). A typical measurement schematic setup is illustrated in Figure 8.

Figure 9a shows the optical spectrum of a typical ETFG from 1200 to 1700 nm, exhibiting unique paired loss peaks due to polarisation mode splitting, when probed using unpolarised BBS. When polarised light with proper polarisation state is launched as a probe, only one set of split modes will be excited and the other set disappears. As can be seen from Figure 9b, either the equivalent fast- (blue dash-dotted line) or the slow-axis (red-dashed line) mode can be fully excited or eliminated with polarised light.

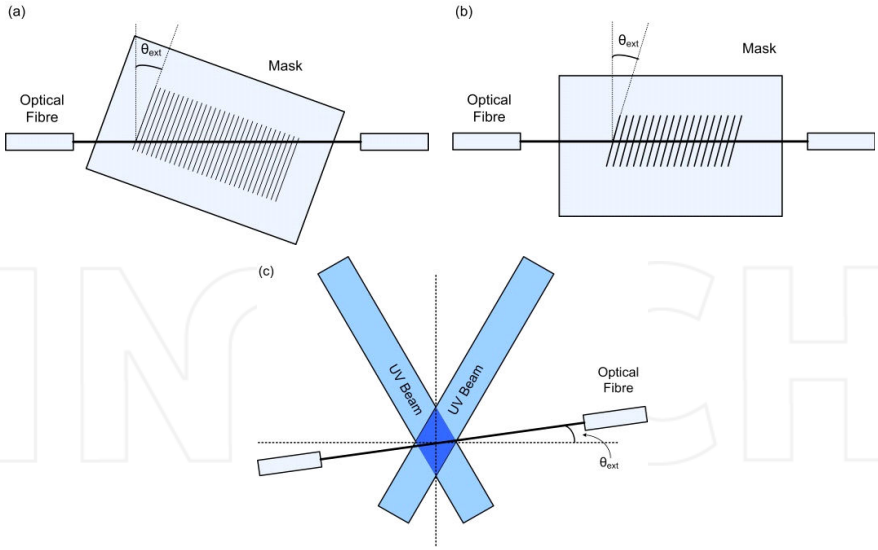

Figure 6. (a) and (b) mask scanning (c) two-beam holographic technique for TFG fabrication.

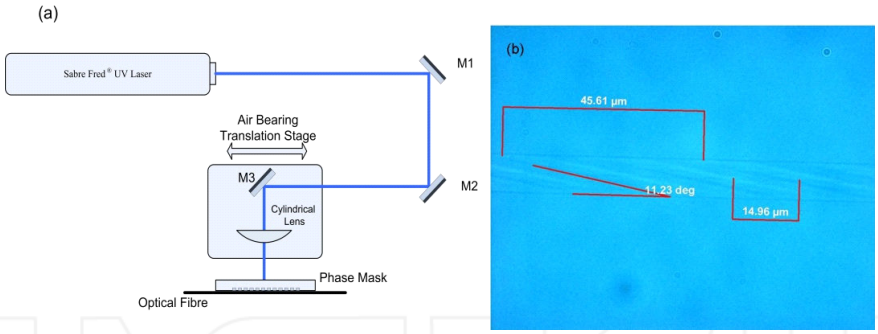

Figure 7. (a) Schematic of UV mask scanning technique for ETFG fabrication; (b) a typical microscopic image of an ETFG (Reprinted from Optics Communication Vol.305 pp271-275, Copyright (2013) with permission from Elsevier).

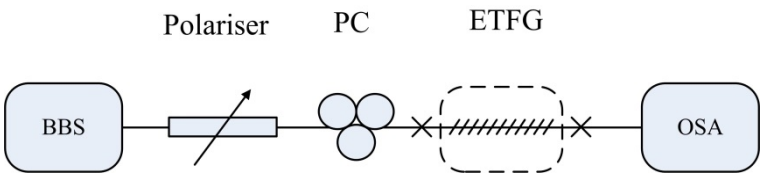

Figure 8. Typical measurement schematic for characterising ETFG.

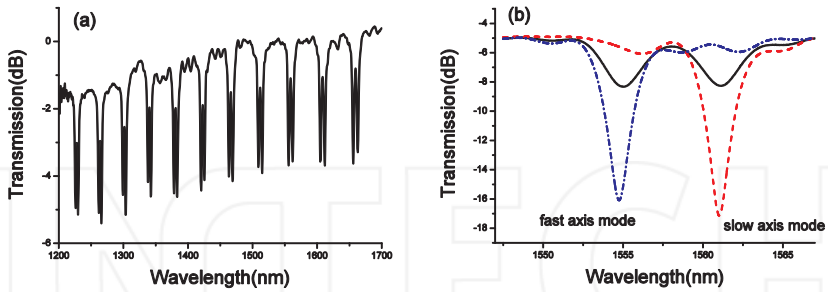

Figure 9. (a) Optical spectrum of a typical ETFG from 1200 nm to 1700 nm; (b) the spectra of one zoomed loss peak pair when polarised light probing the ETFG (Reprinted from Optics Communication Vol.305 pp271-275, Copyright (2013) with permission from Elsevier).

4. Thermal responsivity of ETFG

The ETFGs have shown a thermal responsivity as low as 3.3 pm/°C in 1200 nm range [19]. For the application of optical sensors, the thermal responsivity in the 1550 nm range is of interest. The thermal responsivity of the ETFG has been examined by mounting the grating on a peltier device based heat exchange board using a commercial temperature controller while monitoring the transmission spectrum change with elevated temperature. We studied two pairs of loss peaks of the ETFG around 1560 nm and 1610 nm individually. Figure 10 plots the wavelength shift of the two paired loss peaks when the temperature of the grating increases from 20 °C to 80 °C with a step of 10 °C. Because a polariser and a PC has been used in the experiment, extra insertion loss is therefore induced to the system. Moreover, the BBS has a low power response at the interested wavelength range. Hence, the measured intensity of the loss peaks almost reach the sensitivity limit of the OSA. While the resolution of the OSA used in the experiment was limited to 0.02 nm, the errors in the experiment in terms of wavelength change is 0.04 nm which is shown in the error bars. Figure 10 shows the thermal responsivities of the two paired loss peaks have a quasi linear relationship. The thermal responsivities of the fast- and slow-axis modes around 1560 nm are 4.5 pm/°C and 5.5 pm/°C (Figure 10a) while around 1610 nm are 4.5 pm/°C and 7.5 pm/°C (Figure 10b). It can be clearly seen that the thermal responsivity of ETFG depends on the mode orders, this is quite similar to the thermal behaviour of normal LPGs [20]. We have also found that the thermal responsivity of slow-axis mode is slightly higher than that of the fast-axis mode. Furthermore, compared to the conventional LPG [20], ETFG shows a much lower temperature sensitivity. Therefore, the ETFG could be an ideal optical sensor without compulsory temperature compensation scheme.

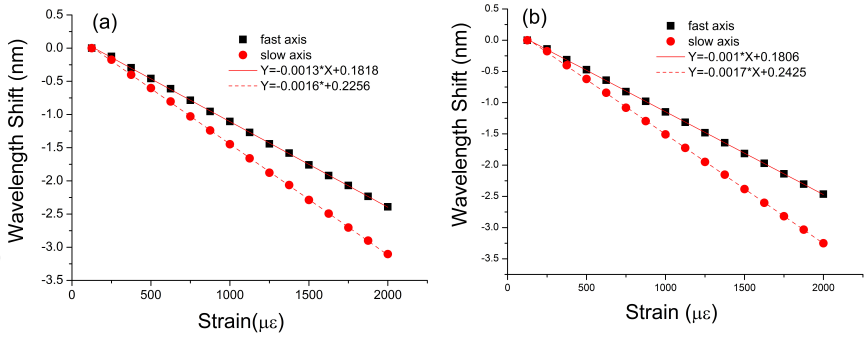

Figure 10. Wavelength shifts of two paired loss peaks of the ETFG against the temperature change in the ranges around (a) 1560 nm and (b) 1610 nm (Reprinted from Optics Communication Vol.305 pp271-275, Copyright (2013) with permission from Elsevier).

5. ETFG based strain sensing

To evaluate the strain responsivity of the ETFG, the grating fibre was mounted in a homemade fibre stretcher where the fibre was clamped on two metal block holders with a fixed distance, one of which being fitted with a precision translational micrometer driver. By moving the micrometer driver, the fibre was then stretched therefore inducing the strain from 0 to 2000 με. Figure 11 depicts the wavelength shift against applied strain for two paired loss peaks. The figure shows a linear relationship between the wavelength change and the applied strain. It can be seen that the strain responsivities of the fast- and slow-axis modes around 1530 nm are 1.3 pm/με and 1.6 pm/με (Figure 11a) while are 1 pm/με and 1.7 pm/με (Figure 11b) in the region around 1610 nm. We notice that the strain responsivity of the ETFG is slightly higher than FBG [3]. The strain responsivity of the fast-axis mode is generally higher than that of the slow-axis mode. It also worth to notice that the resonant wavelength of the ETFG has blue shift while it is under tensile strain. This is in contrast to the FBG strain response, however, corresponds very well to an LPG with relatively small period [20].

Although the passive detection of wavelength shift can offer smart sensing solutions, the systems are still subjected to complexity. Normally, in this case, an additional light source is necessary. Active strain sensors using fibre laser configuration provide an alternative measurement method with higher signal to noise ratio while having a less complicated system. Moreover, most of the passive sensing systems rely on optical spectrum domain signal demodulation from which the cost is high. Time domain signal demodulation offering low system cost has been reported through integrating a conventional LPG in a linear laser cavity [21]. In the following section, we describe the demonstration of a fibre laser strain sensor incorporating an ETFG. Low cost time domain signal demodulation can be achieved by monitoring the built-up time of the modulated laser cavity. The built-up time of the laser system is subject to the loss change of the cavity in a modulated laser system when gain and

pump condition is constant. Because the ETFG has spectral loss bands, when it is subjected to mechanical strain in the laser cavity, the loss band will then shift accordingly, so that the cavity loss is related with applied strain and the built-up time of laser system will change correspondingly. Therefore the strain can be detected by monitoring the built-up time of the laser system.

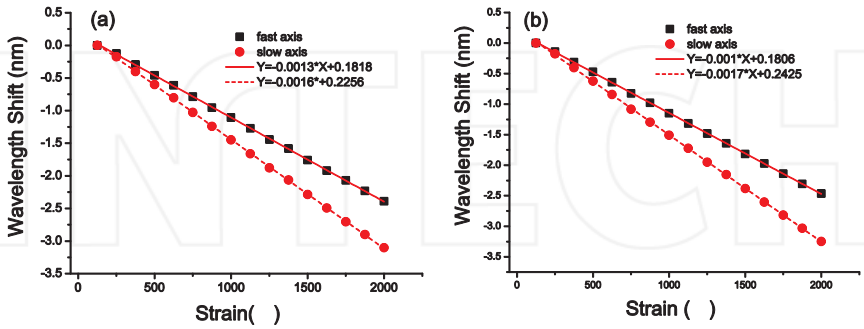

Figure 11. Wavelength shifts of two paired loss peaks of the ETFG against the temperature change in the ranges around (a) 1530 nm and (b) 1620 nm.

The setup for the proposed fibre laser strain sensor system is shown in Figure 12a. The ETFG is again mounted in a home made fibre stretcher. The pump LD is modulated by a square wave through a standard function generator at 5 Hz. The laser output is connected to a low noise photodiode, and the built-up time is measured via a standard two-channel digital oscilloscope. Figure 12b shows a typical oscillation trace of the laser oscillation built-up process.

In the experiment, by tuning the micrometer, we can obtain equivalent strain from 0 με to 2000 με applied on the ETFG. When the ETFG is at 0με, this corresponds to the maximum loss in the laser cavity which gives out the longest built-up time. While the strain increases, the loss bands will have a blue shift thus decreasing the cavity loss which results in a shorter built-up time of the system. A typical output spectra change is illustrated in Figure 13a.

The system was firstly set the lower and upper level modulation pump at constant values of 14.6 mW and 112.4 mW individually. The built-up time was then measured for the strain applied on the ETFG with an increment of 100 με. The absolute built-up time change against the applied strain on the ETFG is depicted in Figure 13b. From Figure 13b it can be seen that, initially when the ETFG is under no strain, the laser cavity suffers the maximum loss therefore exhibiting the largest built-up time. The experiment was then repeated for a different lower pump level at 24 mW. It can also be found that this laser strain sensor system is subject to the saturation of the applied strain as the system is in different lower pump levels. For a better understanding of the experimental results, it has been re-plotted from which linear range of the sensor response counts for in Figure 13b (i.e. lower pump level 24 mW) and Figure 13c (i.e. lower pump level 14.6 mW). It indicates, when the lower pump level is 14.6 mW, the sensor system can measure strain from 0 με to 1000 με

with a linear responsivity of ~500 ns/με. This is far beyond the resolution of a standard oscilloscope. The sensor then reaches its saturation point when the applied strain is over 1000 με. For lower pump level at 24 mW, the sensor is only capable of measuring strain from 0 με to 500 με with a linear strain responsivity of ~349 ns/με.

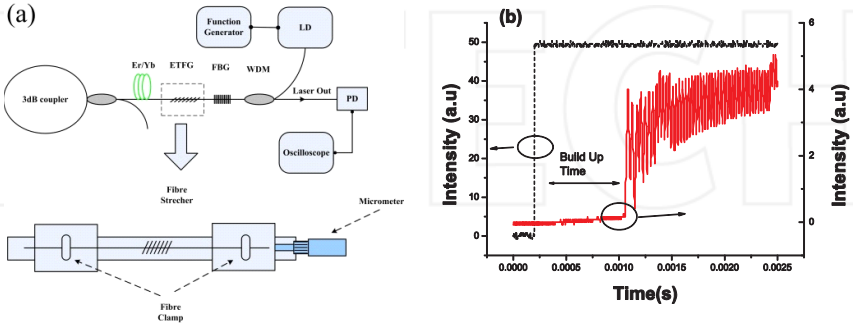

Figure 12. (a) Schematic diagram of the ETFG based fibre laser torsion sensor system; (b) Typical built-up time trace of the fibre laser observed on a digital oscilloscope. Modulation signal is shown in black dotted line; laser output signal is shown in red solid line.

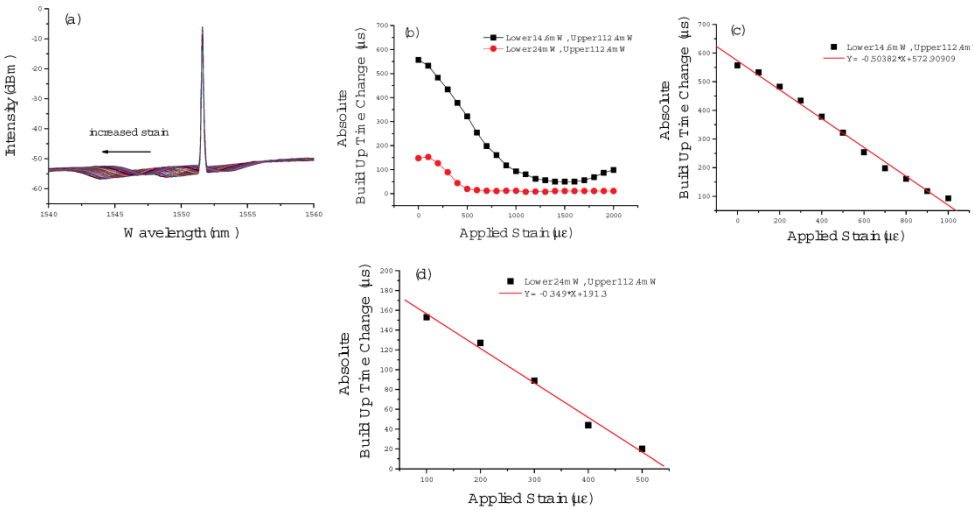

Figure 13. (a) Typical output spectrum change when the 79°-TFG is under strain; (b) Laser oscillation built-up time against applied strain on 79°-TFG for two different lower modulation pump power levels, and re-plotted separately for (c) lower pump level 14.6 mW from 0 to 1000 με (d) lower pump level 24 mW from 0 με to 500 με.

6. ETFG based twist sensing

As the ETFG is polarisation dependent, when probed with polarised light, the polarisation direction of the light will alternate accordingly if the fibre is under twist. The schematic of ETFG twist sensor is shown in Figure 14. In Figure 14, the broadband light is polarised through a fibre pigtailed linear polariser. The PC is then employed to alternate the state of polarisation of the input light to excite either fast-axis or slow-axis mode of the ETFG. One side of the ETFG is clamped on a stage using a metal block while the other side of the ETFG is fed into the OSA through a fibre rotator. The length between the fibre clamp and the fibre rotator is defined as L. A small tension was then applied to the fibre in order to eliminate the axial strain and bending effects, which may induce measurement uncertainty. Before the twist measurement commenced, the zero degree of rotation was normalised to a state that only fast-axis mode is fully excited by adjusting the PC. The twist was then applied to the grating in clockwise direction from 0° to 180° with 10° increment. The resultant transmission spectra evolution is depicted in Figure 15. From Figure 15 one can clearly see that when the ETFG is under twist, the strength of fast-axis mode increases while that of the slow-axis mode decreases. More importantly, the fast-axis mode diminished completely when the twist angle is 180°. A *vice versa* evolution was also observed when the twist was applied in the anti-clockwise direction from 0° to 180° between the fast-axis and slow-axis mode.

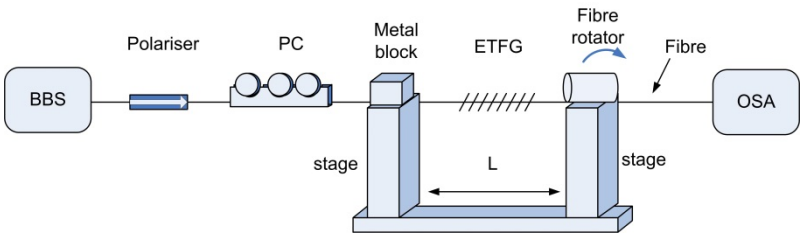

Figure 14. Schematic description of ETFG twist sensor system using a BBS.

In order to make the system more integrated, we carefully spliced the ETFG with a 45°-TFG make the system a compact all-fibre grating based system. While the polarising axis of the 45°-TFG matches either the fast-axis or slow-axis, the corresponding mode will be excited so that the necessity of PC adjustment is removed. To further lower down the cost of the system, single wavelength laser (SWL) was employed as a light source to which the laser line matches either the fast-axis or slow-axis mode. Therefore, while the twist was applied on the ETFG, the power variation can be recorded using a low cost power detector rather than an expensive OSA. The experimental setup of this improved low cost system is shown in Figure 16.

To perform the twist experiment, the SWL is set at the wavelength matching either the fast-axis or slow-axis mode as shown in Figure 17. The zero position of the sensor was calibrated by optimising the fibre rotator which has a minimum transmission power. The twist was then applied again from 0° to 180° with an elevation step of 10° for both fast-axis and slow-axis mode.

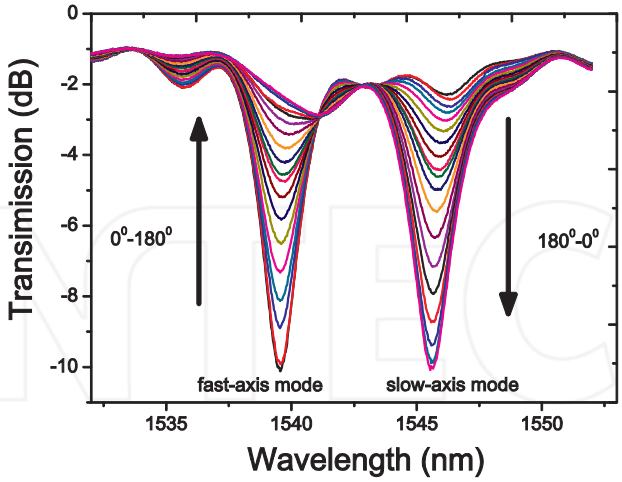

Figure 15. Spectral evolution of ETFG under twist in clockwise direction from 0° to 180° with an increment of 10°.

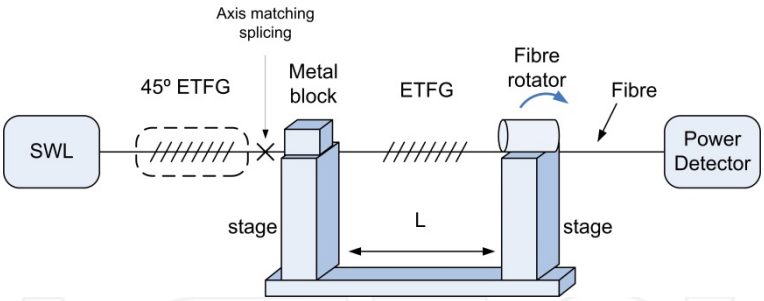

Figure 16. Schematic experimental setup of all-fibre grating based twist sensor system.

The result of the ETFG based twist sensor using power detection method is shown in Figure 18. In Figure 18a, it demonstrates that from 0° to 180° the transmission power of the fast-axis mode increases from -10 dBm to -2 dBm while that of the slow-axis mode is *vice versa*. One may identify a linear range of the sensor at the position of 90°±30°. Thus the sensitivity of the sensor is 0.1 dBm/(rad/m) and 0.24 dBm/(rad/m) for the slow-axis and fast-axis mode respectively. In Figure 18b, it shows similar results when detected with a photodetctor resulting in a voltage change from 0 to 3000 mV. The corresponding linear range gives out a sensitivity of 102.4 mW/(rad/m) and 101.8 mW/(rad/m) for the slow-axis and fast-axis mode individually. It can be seen clearly that when using a photodetector, the linearity is better than using a power meter. Also, the sensitivity is slightly better when using a photodetector. The twist sensitivity of both fast-

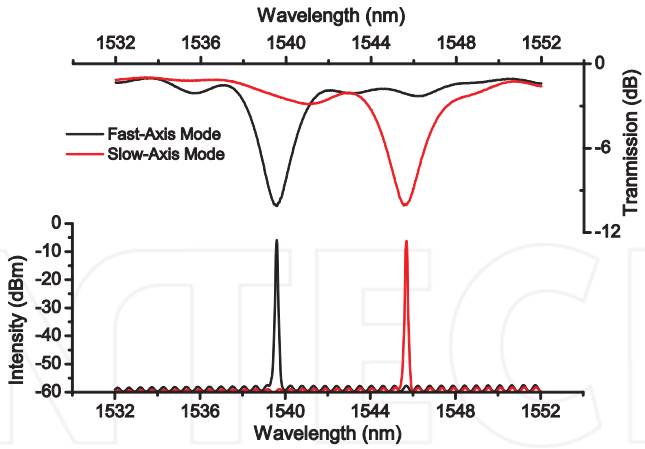

Figure 17. The upper plot is the transmission spectra of the ETFG; the lower one is the output spectra of a SWL set at the wavelength matching either fast-axis or slow-axis mode.

axis and slow-axis mode is quite similar. Therefore, in the real application, either mode can be used. The successful demonstration of using photodetector may provide a mechanism that the signal could be potentially transmitted through wireless control and remote monitoring.

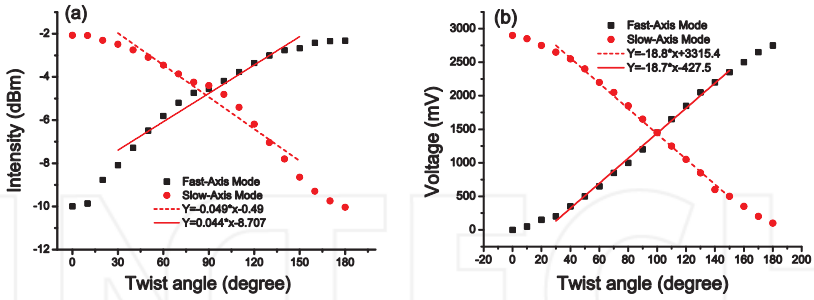

Figure 18. Transmission power variation against twist angle for fast-axis and slow-axis modes measured through low-cost power detection methods: (a) using a power meter and (b) a photodetector.

Similar to strain sensing, the ETFG can also be incorporated into a fibre laser to form a fibre laser based twist sensor system where time domain signal demodulation technique can be applied. The system setup is quite similar to the ETFG based fibre laser strain sensing system, the only difference is to replace the fibre clamps for strain by a set of fibre rotator. The setup for the ETFG based fibre laser twist sensor system is shown in Figure 19. The ETFG itself is a polarisation dependent loss filter, when an ETFG is inserted to the laser cavity and subject to

twist, the intracavity loss will change accordingly, thus affecting the laser built-up time. Based on this principle, the twist experienced by the ETFG can therefore be monitored by measuring the built-up time of the laser cavity.

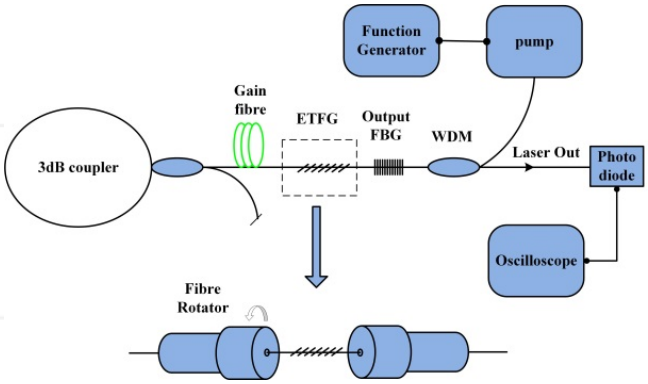

Figure 19. Schematic diagram of the ETFG based fibre laser twist sensor system. (reprint from REF[15] with permission from SPIE).

In the experiment, a segment of laser cavity fibre with ETFG was fixed by a clamp on one side and the other side was mounted on a fibre rotator, as shown in Figure 19a. In order to eliminate the noise induced from other effects such as axial strain and bending, the grating fibre was under small tension to maintain it straight. In the twist sensing experiment, the lower and upper modulation levels of the pump power were first set at 14.6 mW and 43.3 mW, respectively. To perform the measurement, the grating fibre was subjected to twist from 0 to 150° with an elecvation of 10° in both clockwise and anti-clockwise directions. We have measured the built-up time for each twist angle and the normalised results are plotted in Figure 20a. Figure 20a shows that at the initial position, i.e. under 0° twist, the ETFG induced polarisation loss to the laser cavity is at its maximum, so the largest built-up time is expected at this point. Therefore, when the grating fibre is subjected to twist in either clockwise or anti-clockwise direction, the induced polarisation loss through the ETFG to the laser cavity decreases and the built-up time hence reduces accordingly with increasing twist. We have repeated the twist experiment at a different lower pump modulation level of 24 mW. We observed a decrease for the overall torsion sensitivity, as the lower trace shown in Figure 20a. This is because a higher pump power could provide higher gain for the laser system therefore shorter build up time is expected. To work out the sensitivity of the twist sensor, we re-plot the results for twist applied in clockwise and anti-clockwise direction separately in Figure 20b and Figure 20c. Within the dynamic range of ±140°, the sensor shows a quasi-linear response indicating a torsion sensitivity of ~412 μs/(rad/m). The resolution of the oscilloscope used in the experiment is 5 ns, this gives an estimated sensor resolution of ~1.25×10^{-5} rad/m. Furthermore, if the sensor is set at a predefined twist angle, i.e. at ±80° as indicated in Figure 20b and Figure 20c, one is able to identify the twist direction.

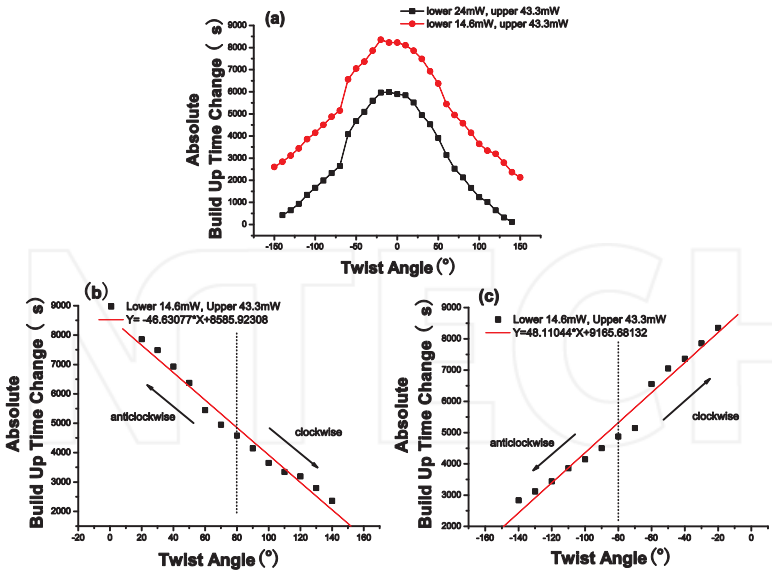

Figure 20. (a) Laser oscillation built-up time against twist angle for twist applied to clockwise and anti-clockwise directions for two different low modulation pump power levels, and re-plotted separately for (b) clockwise and (c) anti-clockwise direction to show the capability of identifying twist direction. (reprint from REF[15] with permission from SPIE).

One may notice that when the torsion angle varies from -140° to 0°, there is a very obvious jump for the built-up time change from -80° to -60°. This could be attributed to the experimental error from rotating the grating in the laser cavity, as there is no such jump for rotation angle from 0° to +140°. To increase the sensitivity of the sensor, it is possible to further decrease the lower modulation pump level.

7. ETFG based loading sensing

Take a standard single mode optical fibre with cylindrical geometry into consideration, when the transverse force is applied to the y axis as shown in Figure 21, for a given compressive force F, the stresses in x and y directions can be expressed as $\sigma_x = \frac{2 \cdot F}{\pi \cdot D \cdot L}$ and $\sigma_y = -\frac{6 \cdot F}{\pi \cdot D \cdot L}$ where D is the diameter of the fibre, L is the length of the stressed area and F is the force applied on the fibre. It is noted that δ_x is tensile stress which is positive while δ_y is compressive stress which is negative therefore $(\delta_x - \delta_y)>0$ is always true. The photoelastic effect induced refractive index change in the fibre core area can be given by [22]:

$$\Delta n = n_x - n_y = \left(n_{x0} - n_{y0}\right) + \left(C_1 + C_2\right) \cdot \left(\delta_x - \delta_y\right) \tag{1}$$

Where n_{x0} and n_{y0} are the effective refractive indices of the fibre without stress. C_1 and C_2 are the stress-optical coefficient, the relationship (C1-C2)>0 is always true for silica fibre [23]. If the transverse load is applied in the slow-axis of an ETFG, we will have $n_{x0}=n_f$ and $n_{y0}=n_s$ where n_f and n_s are the refractive indices for the predefined fast- and slow-axis of the ETFG. Hence, the first term in equation (1) will be negative which will therefore reduce the birefringence Δn. Under this situation, we anticipate the light coupling to the two orthogonal polarised modes is apt to be affected by the external loading. On the contrary, if the transverse load is applied in the fast-axis direction, we will have $n_{x0}=n_s$ and $n_{y0}=n_f$. Therefore, we will have a positive value in the first term of equation (1) which will increase the birefringence Δn. In this scenario, the ETFG is capable of preventing light from coupling to the two orthogonal polarised modes.

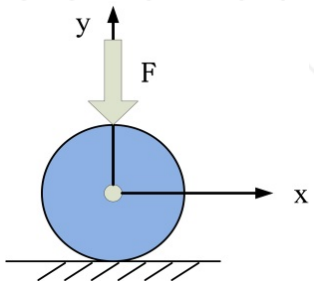

Figure 21. The cross section of a fibre in an assigned *x–y* coordinate system with transverse load applied along the *y*-axis.

The schematic experimental setup of the ETFG loading experiment is shown in Figure 22a. In the experiment, an ETFG with 12 mm length and a support fibre were sandwiched between the flat surface of a buffer plate and a base plate. The loading was applied on top of the buffer plate with a nominal loading length of ~ 32 mm. A BBS was polarised through a commercial polariser, the PC was employed to choose the desired polarisation state, here we choose, the fast-axis mode of the ETFG. The spectral evolution was recorded through an OSA. The applied transverse load on the slow-axis of the ETFG was from 0 to 2600 grams with an increment of 200 grams as shown in Figure 22b. The spectral evolution is plotted in Figure 23. It can be seen clearly from Figure 23 that with the increase of the loading weight, the intensity of the fast-axis mode is elevating while that of the slow-axis mode is decreasing. While we found when the loading is applied on the fast axis of the ETFG as shown in Figure 22c, no spectral evolution can be observed. This unique property could potentially serve as a vectorial loading sensor which is capable of not only measuring the amplitude of the loading but also identifying the direction of the loading.

Similar to the twist sensor, the loading sensor can also be optimised into a low cost sensor using a SWL and optical power detector. There also exists a linear range from 9 to 44 kg/m for the loading responsivity which is approximately 2.04 μW/(kg/m). Therefore, by using a standard detector with 1nW resolution, one could possibly reach a loading sensitivity of 0.0016 grams.

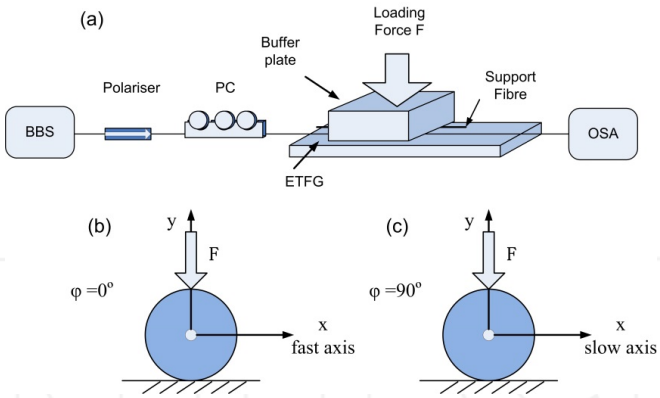

Figure 22. (a) Schematic experimental setup of the transverse loading experiment using an ETFG. (b) and (c) The cross section of the TFBG with transverse load applied along slow- and fast-axes; *φ* is the angle between the fast-axis of the ETFG and the *x* direction.

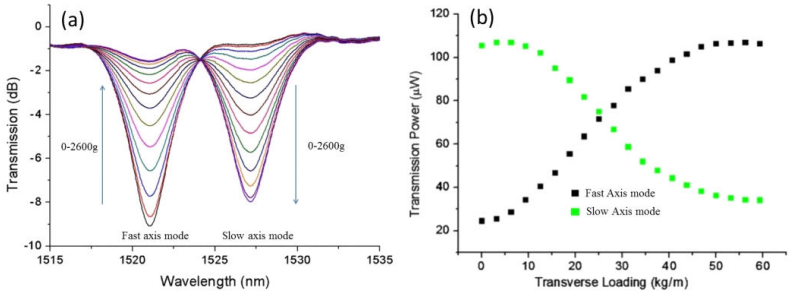

Figure 23. (a)Transmission spectral evolution of the ETFG with transverse load from 0 to 2600g applied on the slow-axis of the ETFG and the support fibre. (b) Power evolution of the ETFG loading sensor using SWL and power meter.

8. ETFG based refractive index sensing

Due to the nature of forward propagating cladding modes, the ETFG is intrinsically sensitive to the external refractive index variation which is similar to an LPG. To characterise the RI responsivity, the ETFG was mounted in a V-grooved aluminium plate, this is to guarantee the measurement being free from other effects such as strain and bend. The refractive index gel used to study the RI response of the ETFG is certified commercial gels from Cargille Lab. The optical spectrum was recorded through a BBS and an OSA to study the spectral evolution of RI response. In Figure 24, it clearly shows the two paired modes around 1560 nm and 1610 nm in response to the RI gels with index change from 1.32 to 1.38 with an increment of 0.01. An obvious trend is the degeneration of the dual loss peaks with increasing RI value. This can be

explained by the reduction of polarisation mode dispersion (PMD) of the cladding modes resulting from the decrease of refractive index difference between the fibre cladding and outer medium. Figure 25a and Figure 25b shows the RI responses of the fast- and slow-axis mode for 1560 nm and 1610 nm band, respectively. It can be clearly seen that the wavelength shift for the two bands is around ~20 nm when the RI increased from 1.32 to 1.38. Additionally, the wavelength shift for 1610 nm band is observed to be slightly larger than that of the 1560 nm band. It is also obvious to see that the ETFG has stronger RI response for the RI value around 1.3 compared to conventional LPGs [20] which does not respond at this RI range. This indicates that ETFG could be an ideal candidate as bio/chemical sensor for water based solutions. Despite the RI response within the desired RI range is not linear, the RI sensitivity of the two peaks is estimated to be ~320 nm/RIU in ~1.33 refractive index region, which is much higher than that of reported typical LPGs [20]. Further increase the RI may result in RI match between the cladding and the index gel. This will remove the boundary condition for the survival of cladding modes, therefore only radiation mode will appear without any loss band structure in the optical spectrum.

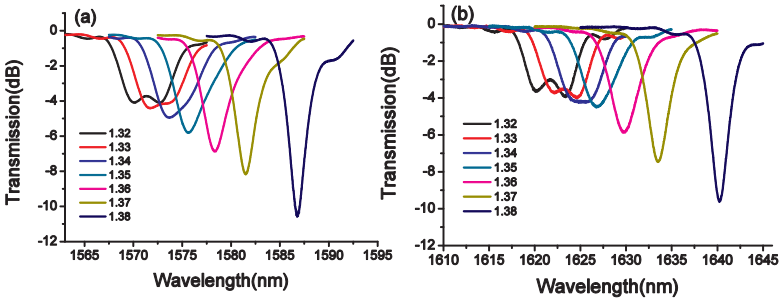

Figure 24. RI response of a mode pair when subject into index gel from RI=1.32 to 1.38 with an increment of 0.01 for (a) 1560 nm band and (b)1610 nm band (Reprinted from Optics Communication Vol.305 pp271-275, Copyright (2013) with permission from Elsevier).

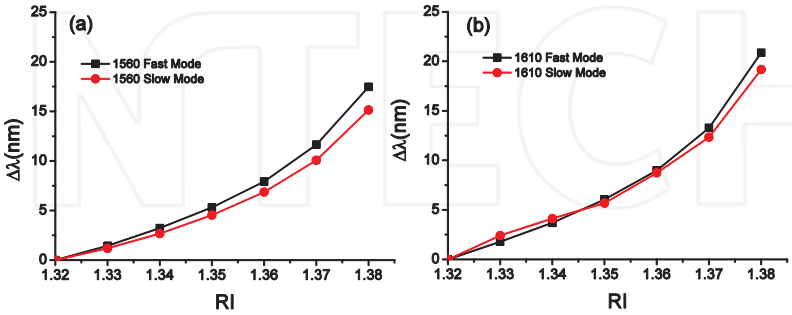

Figure 25. RI response of fast- and slow- axis modes around (a) 1560 nm and (b) 1610 nm when the ETFG was subjected to index gels with SRI change from 1.32 to 1.38 with an increment of 0.01 (Reprinted from Optics Communication Vol.305 pp271-275, Copyright (2013) with permission from Elsevier).

9. Liquid level sensor

Based on the RI response of the ETFG, we notice that when the ETFG is fully immersed in water, the paired peaks shifted to the longer wavelength side, as shown in Figure 26. It is this water induced wavelength shift enables ETFG to be an effective liquid level sensor. If part of an ETFG is immersed in the water, it behaves as two individual gratings with two types of surrounding media. Hence, when we just observe one paired loss peaks, we will see that a paired loss peaks generated by the air-surrounded grating section with a broad peak on longer wavelength side generated by the water-surround grating sections, as illustrated in Figure 26. This behaviour exhibits similarity to LPG and etched FBG based level sensors, and further proves that the effective index of the propagating cladding or core mode is defined by the RI of the surrounding medium covering the waveguide. Owing to the PMD nature of the ETFG cladding modes, we have excited fast- and slow-axis mode individually by polarised light to evaluate the ETFG spectral response to water level change.

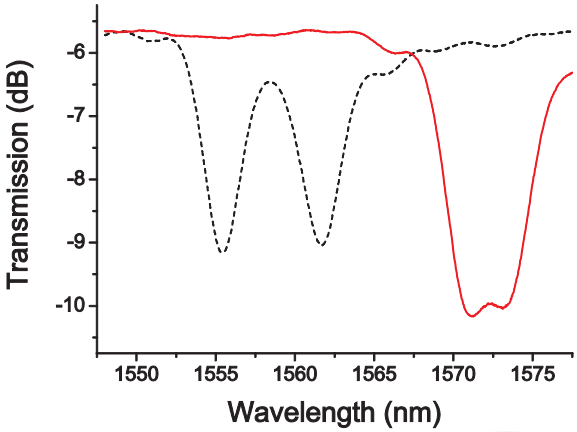

Figure 26. The transmission spectra of a 78°-ETFG when it is in air (black solid line) and fully immersed in water (red dotted line) (Reprinted from Optics Communication Vol.305 pp271-275, Copyright (2013) with permission from Elsevier).

In the water level sensing experiment, a 12 mm long grating was attached to a plastic tube and then immersed into the water. One part of the tube surface was removed to house the grating fibre which is to ensure the grating is in full contact with water while also eliminating the grating from bend. A precision translational stage was used to hold the beaker so that water level on the submerged ETFG can be accurately controlled. Hence during the whole experiment, the fibre movement can be eliminated which stops the polarisation induced uncertainty. Figure 27a describes the schematic configuration of the level sensing experiment. In Figure 27b, it shows the transmission spectra when the slow-axis mode around 1560 nm band was excited at three different liquid levels: the left peak (red solid line) indicates that the grating

fully exposed to air, the middle two peaks (blue dashed line) appear when half of the grating is immersed in water, the right peak (black dotted line) illustrates that the grating is completely immersed in water. The spectral evolution of the slow-axis mode around 1560 nm when the ETFG was surrounded completely from by air to water is illustrated in Figure 27c. It is clear to see that when the water level increases, the loss of the air-surrounded peak decreases whereas the loss of the water-surrounded peak elevates. Figure 27d shows that the fast-axis mode around 1560 nm band exhibited a similar spectral change,

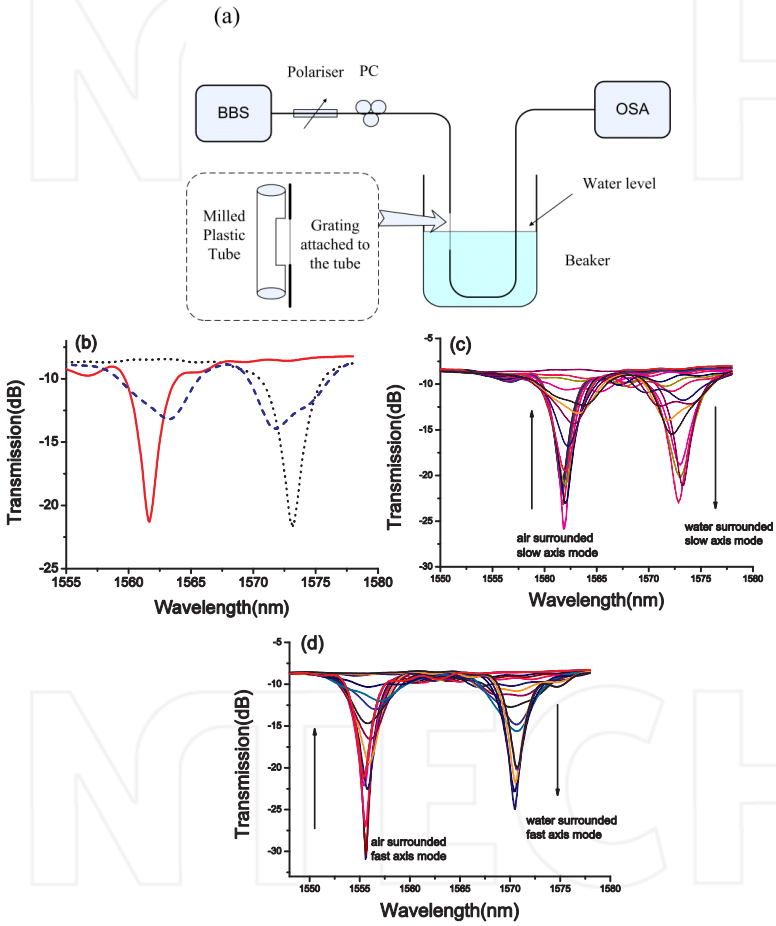

Figure 27. (a) Schematic diagram of the experimental setup for liquid level sensing; (b) Transmission spectra of the ETFG for slow-axis mode coupling around 1560 nm: the left-side (red solid line), right-side (black dotted line) single peak and the middle dual peaks (blue dashed line) corresponding to the grating surrounded by air, water and half way in water. The air- and water-surrounded peaks evolving with increasing water level for (c) slow-axis mode and (d) fast-axis mode (Reprinted from Optics Communication Vol.305 pp271-275, Copyright (2013) with permission from Elsevier).

The transmission against submerging length of the ETFG in water for the fast- and slow-axis mode are depicted in Figure 28a and Figure 28b respectively.

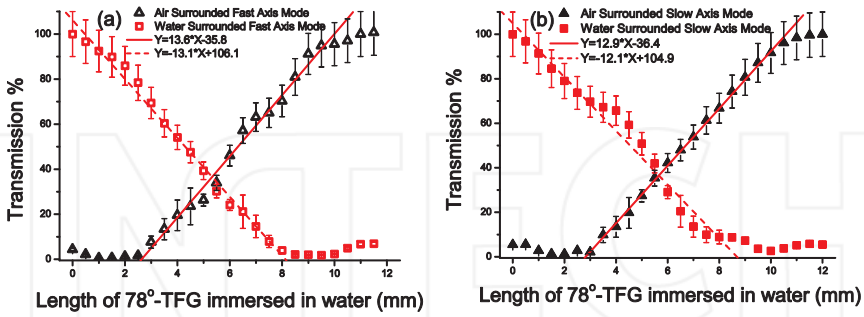

Figure 28. Transmission change measured for the length of the 78-TFG in water for the grating sections surrounded by water (■,□) and by air (▲,△) for (a) fast-axis mode and (b) slow-axis mode (Reprinted from Optics Communication Vol.305 pp271-275, Copyright (2013) with permission from Elsevier).

In Figure 28, it can be seen that by observing the transmission of the fast-axis or slow-axis mode and the related water surrounded peak of the ETFG, we can determine the water level. Additionally, one need to note that the initial 3 mm for the air-surrounded modes is not sensitive to the water level variation. The grating has a linear response to the water level change from 3 mm to 10 mm and becomes insensitive from 10 mm to 12 mm. While for the water-surrounded modes, the grating response has a linear relationship to water level from 0 mm to 8 mm followed by an insensitive range from 8 mm to 12 mm. It is still not clear that why the sensing range is different between the air- and water-surrounded modes. We further linearly fitted the results to characterise the sensitivity of the level sensor.

In Figure 28a, it can be seen the sensitivity for the air-surrounded fast-axis modes is quite similar to that of the water-surrounded one which is ~ 13 %/mm despite the sensing range is different for these two modes. The air- and water-surrounded slow-axis mode show a sensitivity of ~ 12 %/mm which is shown in Figure 28b. This is more than twice of the sensitivity of the LPG based liquid level sensor with a reported value of 4.8 %/mm [24]. We can therefore conclude that both fast- and slow-axis mode of the ETFG is capable of water level sensing which offers similar sensitivity and measurement range. The manufacture quoted accuracy of 7 % (0.3 dB) of the OSA can be regarded as the main factor of measurement uncertainties in the experiment. Also, the environmental effect could be taken into account because the measurement is polarisation sensitive. The uncertainty may increase up to ~ 35 % if the transmission of the water-surrounded mode is getting lower. This is mainly due to reaching the sensitivity limit of the OSA when the transmission of the peaks become smaller. A stronger light source and low loss measurement kit could potentially increase the sensitivity and eliminate these errors. The sensor may also be developed as a low cost solution using single wavelength laser and a power meter.

10. Conclusion

In summary, ETFGs have been demonstrated as effective RI, strain, twist, loading and liquid level sensor. The ETFGs have shown a slightly low thermal responsivity and slightly higher strain responsivity than the standard FBGs. The strain response of the ETFGs is also similar to a short period LPG as shown a negative wavelength shift against strain. Because their unique polarisation mode splitting property, the ETFGs have exhibited vectorial sensing functions as loading and twisting sensors. This allows the ETFG can not only measure the amplitude of the loading and twist but also determine the direction of the measurands. We have described that as a strain or twist sensor, the signal can be demodulated using low cost method with a single wavelength laser and a power detector. Furthermore, we have demonstrated that by incorporating the ETFG in a linear cavity fibre laser, a fibre laser based strain or twist sensor using a time domain signal demodulation method can be realised showing high signal-to-noise ratio for the sensing. The ETFG has also shown strong responsivity to external surrounding medium. Compared to an LPG, the ETFG is sensitive in the RI range ~ 1.33 which allows it to perform efficient sensing for aqueous based solution. Based on this, we have also demonstrated an ETFG based water level sensor with higher sensitivity than an LPG based one.

In the future, we will expect to see more sensor applications based on ETFGs, such as bending sensor and biophotonic application. With proper coating, the ETFGs could function as surface plasmon resonance based ultrahigh sensitivity sensors. So far the theoretical understanding of ETFGs has not been fully realised, thus a systematic study on the theory of the ETFG is expected with which we could find more applications with such unique grating structures.

Author details

Chengbo Mou*, Zhijun Yan, Kaiming Zhou and Lin Zhang

*Address all correspondence to: mouc1@aston.ac.uk

Aston Institute of Photonic Technologies, School of Engineering and Applied Science, Aston University, Aston Triangle, Birmingham, UK

References

[1] Hill KO, Fujii Y, Johnson DC, Kawasaki BS. Photosensitivity in Optical Fiber Waveguides - Application to Reflection Filter Fabrication. Appl Phys Lett. 1978;32(10): 647-9.

[2] Meltz G, Morey WW, Glenn WH. Formation of Bragg Gratings in Optical Fibers by a Transverse Holographic Method. Opt Lett. 1989;14(15):823-5.

[3] Rao YJ. In-fibre Bragg grating sensors. Meas Sci Technol. 1997;8(4):355-75.

[4] Anderson DZ, Mizrahi V, Erdogan T, White AE. Production of in-Fiber Gratings Using a Diffractive Optical-Element. Electron Lett. 1993;29(6):566-8.

[5] Bhatia V, Vengsarkar AM. Optical fiber long-period grating sensors. Opt Lett. 1996;21(9):692-4.

[6] Peupelmann J, Krause E, Bandemer A, Schaffer C. Fibre-polarimeter based on grating taps. Electron Lett. 2002;38(21):1248-50.

[7] Miao YP, Liu B, Zhang H, Li Y, Zhou HB, Sun H, et al. Relative Humidity Sensor Based on Tilted Fiber Bragg Grating With Polyvinyl Alcohol Coating. Ieee Photonic Tech L. 2009;21(7):441-3.

[8] Caucheteur C, Chen C, Albert J, Mégret P. Use of weakly titled fiber Bragg gratings for strain sensing purposes. Proc of IEEE/LEOS Benelux Chapter, Eindhoven. 2006:61-4.

[9] Guo T, Tam HY, Krug PA, Albert J. Reflective tilted fiber Bragg grating refractometer based on strong cladding to core recoupling. Opt Express. 2009;17(7):5736-42.

[10] Shao LY, Xiong LY, Chen CK, Laronche A, Albert J. Directional Bend Sensor Based on Re-Grown Tilted Fiber Bragg Grating. J Lightwave Technol. 2010;28(18):2681-7.

[11] Shevchenko YY, Albert J. Plasmon resonances in gold-coated tilted fiber Bragg gratings. Opt Lett. 2007;32(3):211-3.

[12] Mihailov SJ, Walker RB, Stocki TJ, Johnson DC. Fabrication of tilted fibre-grating polarisation-dependent loss equaliser. Electron Lett. 2001;37(5):284-6.

[13] Zhou KM, Simpson G, Chen XF, Zhang L, Bennion I. High extinction ratio in-fiber polarizers based on 45 degrees tilted fiber Bragg gratings. Opt Lett. 2005;30(11): 1285-7.

[14] Zhou KM, Zhang L, Chen XF, Bennion I. Optic sensors of high refractive-index responsivity and low thermal cross sensitivity that use fiber Bragg gratings of > 80 degrees tilted structures. Opt Lett. 2006;31(9):1193-5.

[15] Mou C, Zhou K, Suo R, Zhang L, Bennion I, editors. Fibre laser torsion sensor system using an excessively tilted fibre grating and low-cost time domain demodulation. 20th International Conference on Optical Fibre Sensors; 2009 Oct 5-9; Edinburgh,UK2009.

[16] Chen X, Zhou K, Zhang L, Bennion I. In-fiber twist sensor based on a fiber Bragg grating with 81 degrees tilted structure. Ieee Photonic Tech L. 2006;18(21-24):2596-8.

[17] Suo R, Chen XF, Zhou KM, Zhang L, Bennion I. In-fibre directional transverse loading sensor based on excessively tilted fibre Bragg gratings. Meas Sci Technol. 2009;20(3):034015.

[18] Mou C, Zhou K, Yan Z, Fu H, Zhang L. Liquid level sensor based on an excessively tilted fibre grating. Opt Commun. 2013;305:271-5.

[19] Zhou KM, Zhang L, Chen XF, Bennion I. Low thermal sensitivity grating devices based on Ex-45 degrees tilting structure capable of forward-propagating cladding modes coupling. J Lightwave Technol. 2006;24(12):5087-94.

[20] James SW, Tatam RP. Optical fibre long-period grating sensors: characteristics and application. Measurement Science and Technology. 2003;14:R49-R61.

[21] Yang XF, Luo SJ, Chen ZH, Ng JH, Lu C. Fiber Bragg grating strain sensor based on fiber laser. Opt Commun. 2007;271(1):203-6.

[22] Gafsi R, El-Sherif MA. Analysis of induced-birefringence effects on fiber Bragg gratings. Opt Fiber Technol. 2000;6(3):299-323.

[23] Imoto N, Yoshizawa N, Sakai JI, Tsuchiya H. Birefringence in Single-Mode Optical Fiber Due to Elliptical Core Deformation and Stress Anisotropy. Ieee J Quantum Elect. 1980;16(11):1267-71.

[24] Khaliq S, James SW, Tatam RP. Fiber-optic liquid-level sensor using a long-period grating. Opt Lett. 2001;26(16):1224-6.

INTECH